



HAL
open science

Unequal anthropogenic enrichment of mercury in Earth's northern and southern hemispheres

Chuxian Li, Jeroen Sonke, Gael Le Roux, Natalia Piotrowska, Nathalie van Der Putten, Stephen Roberts, Tim Daley, Emma Rice, Roland Gehrels, Maxime Enrico, et al.

► **To cite this version:**

Chuxian Li, Jeroen Sonke, Gael Le Roux, Natalia Piotrowska, Nathalie van Der Putten, et al.. Unequal anthropogenic enrichment of mercury in Earth's northern and southern hemispheres. 2020. hal-02990211

HAL Id: hal-02990211

<https://hal.science/hal-02990211>

Preprint submitted on 10 Nov 2020

HAL is a multi-disciplinary open access archive for the deposit and dissemination of scientific research documents, whether they are published or not. The documents may come from teaching and research institutions in France or abroad, or from public or private research centers.

L'archive ouverte pluridisciplinaire **HAL**, est destinée au dépôt et à la diffusion de documents scientifiques de niveau recherche, publiés ou non, émanant des établissements d'enseignement et de recherche français ou étrangers, des laboratoires publics ou privés.

Unequal Anthropogenic Enrichment of Mercury in Earth's Northern and Southern Hemispheres

Chuxian Li, Jeroen E. Sonke,* Gaël Le Roux, Natalia Piotrowska, Nathalie Van der Putten, Stephen J. Roberts, Tim Daley, Emma Rice, Roland Gehrels, Maxime Enrico, Dmitri Mauquoy, Thomas P. Roland, and François De Vleeschouwer



Cite This: <https://dx.doi.org/10.1021/acsearthspacechem.0c00220>



Read Online

ACCESS |



Metrics & More



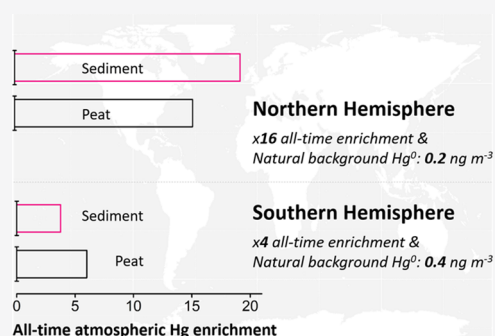
Article Recommendations



Supporting Information

ABSTRACT: Remote Northern Hemisphere (NH) and Southern Hemisphere (SH) lake sediment and peat records of mercury (Hg) deposition have shown a $\times 3$ to $\times 5$ Hg enrichment since pre-industrial times (<1880 AD), leading to the perception that global atmospheric Hg enrichment is moderate and uniform across the hemispheres. Anthropogenic Hg emissions in the NH are, however, approximately 4 times higher than those in the SH. Here, we reconstruct atmospheric Hg deposition in four remote SH peatlands and review sediment and peat Hg records from both hemispheres. We observe a $\times 4$ all-time enrichment in SH Hg deposition from pre-anthropogenic (<1450 AD) to the late 20th-century periods, which is lower than the large $\times 16$ all-time enrichment in NH Hg deposition. We attribute this difference to lower anthropogenic Hg emissions in the SH, and higher natural atmospheric SH Hg concentrations, supported by $\times 2$ higher natural background Hg accumulation in SH peat records. We suggest that the higher SH natural atmospheric Hg deposition reflects the SH land–ocean distribution, and is driven by important SH marine Hg emissions. Our findings indicate that atmospheric Hg background levels and anthropogenic enrichment in both hemispheres are different and should be taken into account in international Hg assessments and environmental policy.

KEYWORDS: mercury, enrichment, peat, sediment, archive, hemisphere, deposition



INTRODUCTION

Mercury (Hg) is a toxic trace metal that affects wildlife and human health.^{1–4} Hg is discharged into the environment by natural processes, such as volcanism, chemical and physical weathering, and by human activities, including mining, coal burning, and intentional use.^{5–7} Elemental Hg⁰, the dominant form of emissions, has a long atmospheric residence time of 6–12 months, which allows for its intrahemispheric dispersion before being deposited to the Earth's surface, including remote environments.⁸ Assessments of the extent of global Hg pollution have relied upon natural archives of Hg accumulation (e.g., sediment,^{9,10} peat,¹¹ ice cores¹²) and on estimates of natural and anthropogenic Hg emissions.⁷

Since early work on lake sediment cores in the 1970s,¹³ hundreds of remote ²¹⁰Pb-dated sediment cores have documented an approximate 3- to 5-fold increase in Hg accumulation rates (HgAR) from pre-industrial (1760–1880 AD) times to the late 20th century.^{14–19} A comprehensive review in 2007 concluded that sediment records were more reliable than peat records in recording atmospheric HgAR.¹⁷ Inferred higher Hg accumulation in peat records was thought to be related to ²¹⁰Pb mobility and peat mass loss during remineralization. A recent review study¹⁸ indicated that earlier peat vs sediment comparisons¹⁷ used different reference

periods to calculate Hg enrichment. Using coherent reference periods, dozens of peat archives and a small number of glacier ice cores also document 3- to 5-fold enrichment factors, similar to sediment records, since pre-industrial times (EF_{preind}).^{14,18} Both sediment and peat records have strengths and weaknesses, with ²¹⁰Pb and Hg mobility during sediment diagenesis and peat decomposition being potential factors of bias.^{20–22} Yet, both archives at remote locations record broadly similar Hg accumulation profiles throughout the past millennium, despite differences in archive functioning, and therefore warrant further comparison across Earth's two hemispheres. Regarding archive functioning, lake sediments integrate Hg deposition across a larger watershed, transient Hg storage in soils, followed by Hg runoff and in-lake cycling, leading to a longer Hg residence time before deposition into sediments. Peatlands integrate Hg deposition directly from the

Received: August 13, 2020

Revised: October 16, 2020

Accepted: October 19, 2020

atmosphere,^{18,23,24} leading to a more direct response of peat archives to atmospheric Hg⁰ concentrations. This can generally be recognized by the 2-fold drop in HgAR from the 1970s to the 1990s in peat,¹⁸ which is absent in sediment records and which mirrors the well-documented decrease in Hg emissions and observed atmospheric Hg⁰ concentrations.^{7,25,26} A comparison of Hg stable isotope composition of peat and lake sediments indicates that in both archives, 75% of Hg derives from the uptake of atmospheric Hg^{0,23} which further justifies comparing both archives.

Longer radiocarbon-dated NH sediment and peat cores record changes in the natural background Hg accumulation during precolonial times (pre-1450 AD), before large-scale mining practices, and indicate a more dramatic difference in Hg deposition. Millennial sediment and peat records show that HgAR already increased 5-fold during the earlier transition from pre-large-scale mining to precolonial times around approximately 1450 AD.¹⁸ As a consequence, all-time anthropogenic Hg enrichment factors (EF_{alltime}, the ratio of the 20th-century to pre-1450 AD HgAR) determined from sediment and peat records range from 16 to 26.¹⁸ The cause for the increase in NH Hg enrichment around 1450 AD has been debated. Some Hg inventory and modeling studies have argued for enhanced Hg emissions from Spanish colonial silver and gold mining.^{27–29} Other studies argue that Hg associated with mining has been immobilized in mining waste, rather than volatilized.^{1,9,30} A study on Hg stable isotopes in peat has recently shown evidence on how enhanced deforestation during the Middle Ages may have impacted regional atmospheric Hg dynamics in Europe with lower vegetation uptake of Hg and wood burning emissions leading to enhanced atmospheric Hg concentrations and deposition.²⁵ What nearly all of the above cited studies have in common is that they are situated in the northern hemisphere (NH) where the majority of historical anthropogenic Hg emissions and studies have taken place. Relative to the NH, anthropogenic Hg emissions in the SH have continuously been 4 times lower.³¹ Reviews of anthropogenic Hg enrichment in the environment generally provide a global picture without differentiating between the hemispheres.^{20,32–34} Lake sediment records of Hg accumulation have been studied in the SH and are reviewed here. Three Southern Hemisphere (SH) peat records have been studied for HgAR^{35,36} but are all incomplete (see [Materials and Methods](#) and [Extended Data 2](#)) and preclude a rigorous assessment of SH atmospheric Hg enrichment based on both sediment and peat archives.

The aim of this study is therefore to investigate potential differences in anthropogenic Hg enrichment in Earth's SH and NH. We hypothesize that, in regard to the lower historical SH anthropogenic Hg emissions, enrichment will also be lower. We extend the limited number of peat archives studied in the SH by investigating Hg accumulation rates in four new radiocarbon and ²¹⁰Pb and ¹⁴C bomb-pulse-dated SH peat records. We then review all of the existing SH sediment and peat HgAR ([Extended Data 2](#)), compare Hg enrichment factors to the NH, and discuss findings in the context of revised volcanic Hg emissions, published historical anthropogenic Hg emissions, and Hg cycling in both hemispheres. We do not include glacier ice cores in our review due to the limited number of studies available. Four reference time periods, operationally defined for NH natural archives elsewhere,^{18,19} will be used throughout: natural background (pre-1450 AD), pre-industrial period (1450–1880 AD), 20th-

century extended HgAR maximum (20Cmax, approximately from 1940 to 1990; see also [Materials and Methods](#)), and the recent post-1990 modern period.

■ MATERIALS AND METHODS

Study Sites. We investigate four new cores from remote ombrotrophic peatlands in the SH mid-latitudes: Amsterdam Island (AMS, S-Indian Ocean), Falkland Islands (SCB, San Carlos bog, Islas Malvinas, S-Atlantic Ocean), and Andorra and Harberton (AND, HBT, Tierra del Fuego, Argentina) (SI Appendix [Table S1](#), [Figure S1](#), [Text S1](#), and [Extended Data 1](#)). These four sites are situated in the southern westerly wind belt, far away from anthropogenic Hg sources, which makes them ideal recorders of SH remote atmospheric Hg deposition trends. Details about the field campaigns and sampling sites are given in SI Appendix [Table S1](#) and [Text S1](#). After collection, all of the cores were photographed, described, and packed in plastic film and PVC tubes and shipped to EcoLab, Toulouse, France. There, the cores were cut and processed following published trace-metal clean protocols, freeze-dried, and stored dry until analysis.^{37,38}

Chronology. Age model output of the AMS peat core is adopted from ref 39. In brief, a total of 20 samples were picked for plant macrofossils and subsequently radiocarbon-dated at the LMC14 Artemis Laboratory (Saclay, France, SacA code) or GADAM center (Gliwice, Poland, GdA code). Recent age control in the AMS peat core is based upon 4 post-bomb radiocarbon dates⁴⁰ together with ²¹⁰Pb dating using the constant rate of supply model, and ¹³⁷Cs, ²⁴¹Am.⁴¹ A total of 9 samples of plant macrofossils/charcoal from SCB, 10 *Sphagnum* macrofossils from AND, and 13 *Sphagnum* macrofossils from HBT were radiocarbon-dated. These radiocarbon samples were pretreated and graphitized at the GADAM center (Gliwice, Poland, GdA code).⁴² Subsequently, their ¹⁴C concentration in graphite was measured at the DirectAMS Laboratory (Bothell, WA⁴³). The NIST Oxalic Acid II standard was used for normalization, and black coal was used as a blank. A total of 22 samples from the top 62 cm of the SCB peat core were selected for ²¹⁰Pb measurement by α counting to constrain the recent age (see [Extended Data 1](#)). The recent age control of the AND and HBT peat cores derive from 5 and 10 post-bomb radiocarbon dates, respectively.^{40,44}

Details of radiocarbon dates are summarized in SI Appendix [Table S2](#). Age-depth models were generated from a combination of radiocarbon dating, post-bomb, and ²¹⁰Pb dating with the Bacon package within R software,⁴⁵ using the SHCal13 calibration curve for positive ¹⁴C ages,⁴⁶ while the post-bomb radiocarbon dates were calibrated with SH zone 1–2 curve.⁴⁷ The prior settings and model outputs are presented in SI Appendix [Figure S2](#). The modeled median age was used for calculating and plotting HgAR against time ([Figure 1](#)). The average age uncertainties (1- σ) derived from the age-depth models range from 1 to 5 years for the topmost part of the cores, up to ca. 100 years around 1000 AD. The investigated peat profiles of AMS, SCB, AND, and HBT cover periods of 6600, 2000, 200, and 800 years, respectively. The corresponding mean peat accumulation rates are 0.76, 0.85, 3.6, and 0.91 mm year⁻¹.

Peat Hg Accumulation Rates (HgAR). HgAR were calculated as the product of Hg concentration (ng g⁻¹), peat density (g cm⁻³), and peat mass accumulation rate (g m⁻² year⁻¹). Peat density was determined for each 1 cm slice by measuring its volume using a Vernier caliper and dry peat mass

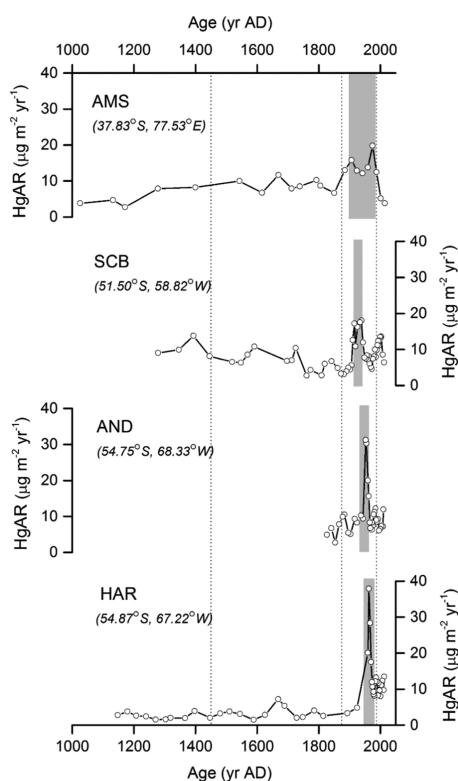


Figure 1. Profiles of Hg accumulation rates (HgAR) in the peat cores from Amsterdam Island (AMS), Falkland Islands (SCB, Islas Malvinas), and Andorra and Harberton (AND, HBT, Tierra del Fuego). The vertical dashed lines operationally separate the natural background (pre-1450 AD), pre-industrial (1450–1880 AD), the extended 20th-century maximum HgAR (20Cmax, gray bars) and modern (post-1990 AD) reference periods, following ref 15.

after freeze-drying. Peat samples were analyzed for total Hg (THg) concentration on a combustion cold vapor atomic absorption spectrometer (CV-AAS, Milestone DMA-80) at the University of Toulouse, France. The IPE 176 CRM (Reed/*Phragmites communis*), NIST 1632d (Coal), and BCR 482 (Lichen) were analyzed with mean recoveries ranging from 93 to 100% (SI Appendix Table S3). Replicate/triplicate analyses of THg in peat samples were found to vary by less than 6% (1σ). Profiles of peat Hg concentration in AMS, SCB, AND, and HBT are shown in SI Appendix Figure S5. Peat mass accumulation rate was determined from the age models and dry peat mass. All raw data are summarized in Extended Data 1.

Literature Review, Reference Time Periods, and Statistics. We expand on a previous literature review of sediment and peat Hg archives.¹⁸ We examined the remote HgAR records from SH lake sediments and peat records in southern South America, lake sediments in New Zealand, lake sediments in East Africa, and lake sediments in Antarctica (see Extended Data 2 for details). We exclude from our analysis: a lake sediment core 6 km downstream from the Potosi mine (Bolivia) with pronounced local mining influences on HgAR;⁴⁹ a lake sediment core in the Patagonian volcanic zone with multiple tephra layers associated with high HgAR.⁵⁰ Two remote Bolivian cores and one Peruvian core also showed evidence for the release of Hg due to regional Spanish colonial mining activities,^{36,51} but are retained in Extended Data 2. Extended Data 2 indicates which records were only partially

used, often due to lack of recent ^{210}Pb or ^{14}C bomb pulse dates. This applies in particular to three SH peat records, where one lacks a recent ^{210}Pb and recent ^{14}C chronology and therefore 20Cmax and pre-industrial HgAR,³⁶ one lacks pre-1988 layers,⁴⁸ and one is nearly complete,³⁵ except for the 1826–1935 period, which we extrapolate (see Extended Data 2).

We use four reference time periods, based on previous studies and originally derived for NH natural archives:¹⁸ natural background (pre-1450 AD), pre-industrial period (1450–1880 AD), 20th-century extended HgAR maximum (20Cmax, approx. 1940–1990), and the recent, modern period (post-1990 AD). For each published study, we calculate mean HgAR during the four reference intervals. The operational cutoff years, e.g., 1450, 1880, and 1990, represent the timing of changes in HgAR observed in NH sediment ($n = 49$) and peat cores ($n = 19$) reviewed here. Note that each archive and each regional context shows variation in the exact timing of gradual or abrupt increases (~ 1450 , ~ 1880) or decreases (~ 1990) in HgAR (Extended Data 2). Several long SH sediment records include the effect of climate change on variations in HgAR during the Holocene and since the last glacial maximum. Depending on watershed type and location, these studies document substantial natural variability in HgAR that is beyond the scope of this study, but no less important. Therefore, to assess, to the best of our ability, the impact of humans on recent millennial atmospheric Hg enrichment, we integrated natural background HgAR between on average -1700 BC and 1450 AD, but on occasion as far back as 10 000 BC (Extended Data 2). We define enrichment factors (EF) based on the evolution of mean HgAR during the four reference periods as follows:

$$\text{EF}_{\text{preind}} = \text{HgAR} (20\text{Cmax}) / \text{HgAR} (\text{pre-industrial})$$

$$\text{EF}_{\text{alltime}} = \text{HgAR} (20\text{Cmax}) / \text{HgAR} (\text{natural background})$$

$$\text{EF}_{\text{p/b}} = \text{HgAR} (\text{pre-industrial}) / \text{HgAR} (\text{natural background})$$

$$\text{EF}_{\text{mod/bck}} = \text{HgAR} (\text{modern}) / \text{HgAR} (\text{natural background})$$

Statistical descriptions are parametric (mean, standard deviation (SD)) for normally distributed HgAR and EF, and non-parametric (median, Q25% and Q75% quartiles, interquartile range (IQR)) for non-normally distributed HgAR and EF. Outlier tests were performed only on EFs, and observations were excluded (in *italics* in Extended Data 2) when they exceeded $2 \times \text{SD}$ around the mean, or $1.5 \times \text{IQR}$ around Q25% and Q75%. All data generated or analyzed during this study are included in the SI Appendix.

RESULTS AND DISCUSSION

New Southern Hemisphere Peat Records. HgAR profiles in the four SH peat records show maximum values during the 20th century (Figure 1). Natural background (pre-1450 AD) HgAR in the HBT, SCB, and AMS cores shows a mean of $4.9 \pm 3.5 \mu\text{g m}^{-2} \text{year}^{-1}$ (mean, 1σ , $n = 33$ in 3 cores; Figure 1). Pre-industrial HgAR in the four cores averages $5.9 \pm 2.5 \mu\text{g m}^{-2} \text{year}^{-1}$, 20Cmax HgAR is $20 \pm 7.9 \mu\text{g m}^{-2} \text{year}^{-1}$, and modern HgAR is $9.7 \pm 2.9 \mu\text{g m}^{-2} \text{year}^{-1}$ (means, 1σ , $n = 4$, Figure 1). AND and HBT have more pronounced 20Cmax peaks than SCB and AMS, which is due to a combination of peaks in Hg concentration (Figure S5) and enhanced peat mass accumulation rate occurring simultaneously (Extended Data 1). While absolute HgAR for the different time periods vary between cores, the relative HgAR changes between cores are similar and can be expressed by enrichment factors (EFs). The four SH cores show evidence for 3.1-fold (mean, $1\sigma = 1.6$)

enhanced net Hg deposition during the 20Cmax, compared to the pre-industrial period (EF_{preind} , Table 1), which at first sight

Table 1. Hg Accumulation Rate (HgAR) Enrichment Factor Observed in the Peat Profiles from This Study^a

	pre-ind/background ($EF_{\text{p/b}}$)	20Cmax/pre-ind (EF_{preind})	20Cmax/background (EF_{alltime})
AMS	1.6	1.7	2.7
SCB	0.6	2.5	1.5
AND		3.0	
HBT	1.4	5.3	7.3

^aAMS, Amsterdam Island; SCB, the Falkland Islands; AND, HBT, Andorra, and Harberton, Argentina. “Pre-ind,” pre-industrial; “20Cmax,” extended 20th-century maximum HgAR (see Materials and Methods); “p/b,” pre-industrial/background.

appears similar to NH natural archives. SH historical HgARs have thus far been studied in 20 lake sediment and 3 peat cores (see Materials and Methods and Extended Data 2 for a full list). Figure 2 summarizes HgAR and EFs in all published SH sediment and peat records, as well as updated NH data for the reference periods of interest (Extended Data 2). The temporal evolution of HgAR in peat and sediment cores is similar between the NH and SH in a broad sense (Figure 2a,b). HgAR increase stepwise from natural background to pre-industrial and then to 20Cmax periods in both sediment and peat archives. Similar to NH peat records,¹⁸ modern-day (post-1990) HgAR in SH peat decrease by a factor of 2 from 20Cmax values (SI Appendix Figure S4), in line with declining global anthropogenic Hg emissions and deposition from the 1970s to 2000s (Figure S6^{25,26}). Sediment records in both the NH and SH do not record this decrease (Figure S4), presumably due to the longer residence of Hg in lake catchment soils, leading to a slower recovery of Hg concentrations in soil runoff into lakes.¹⁸

Hemispheric Trends in Historical Hg Enrichment. The historical evolution of trends in hemispheric HgAR is shown in

EF_{preind} and EF_{alltime} diagrams (Figure 2c,d). Pre-industrial to 20Cmax enrichment in HgAR (EF_{preind}) is higher in peat compared to sediment in both NH and SH (Kruskal–Wallis test, NH, $P = 0.01$; SH, $P = 0.10$). EF_{preind} is higher in the NH than in the SH for sediment (3.1 vs 1.8), but not peat (4.6 vs 3.1; Kruskal–Wallis test, peat, $P = 0.15$; sediment $P = 0.001$; Figures 2c,d and 3a). We find in particular that in long millennial NH records, HgAR increased 3.9-fold in peat and 3.7-fold in sediments across the natural background to pre-industrial periods around 1450 AD ($EF_{\text{p/b}}$, Figure 2c,d and Table 2). In contrast, $EF_{\text{p/b}}$ in SH millennial records show negligible, mean 1.2-fold enrichment in peat to a small, median 1.4-fold enrichment in sediments across the natural background (<1450 AD) to pre-industrial periods. Consequently, all-time NH enrichment factors (EF_{alltime}) reach 16 in peat and 13 in sediments and are larger than the 6.0-fold and 3.8-fold Hg all-time enrichment in SH peat and sediments (Table 2 and Figure 3B; Kruskal–Wallis test, $P = 0.02$ for peat, $P = 0.09$ for sediment). Historical Hg emission inventory and associated box modeling studies have suggested that the 4-fold increase in NH HgAR around 1450 AD is related to Spanish colonial Hg and silver mining.^{7,27} This interpretation has been questioned by studies arguing that the associated emissions are over-estimated.^{1,9,52} SH archives show little evidence of Spanish colonial mining impacts in South America on large-scale SH atmospheric Hg deposition (Figure 2). Similarly, neither NH peat nor sediment records show evidence of a pronounced late 19th-century peak in HgAR, in contrast to large estimated North American gold-rush Hg emissions.⁷ Across the natural background and pre-industrial reference periods, the world’s global population increased 5-fold from 0.22 to 1.2 billion.⁵³ We therefore suggest that the 4-fold NH increase in HgAR around 1450 AD is more likely related to demography-driven changes in land use and associated Hg emissions and deposition (e.g., deforestation,²⁵ wood and peat combustion, urbanization), than to direct Spanish colonial mining emissions of Hg to the global pool. More research is needed to explore

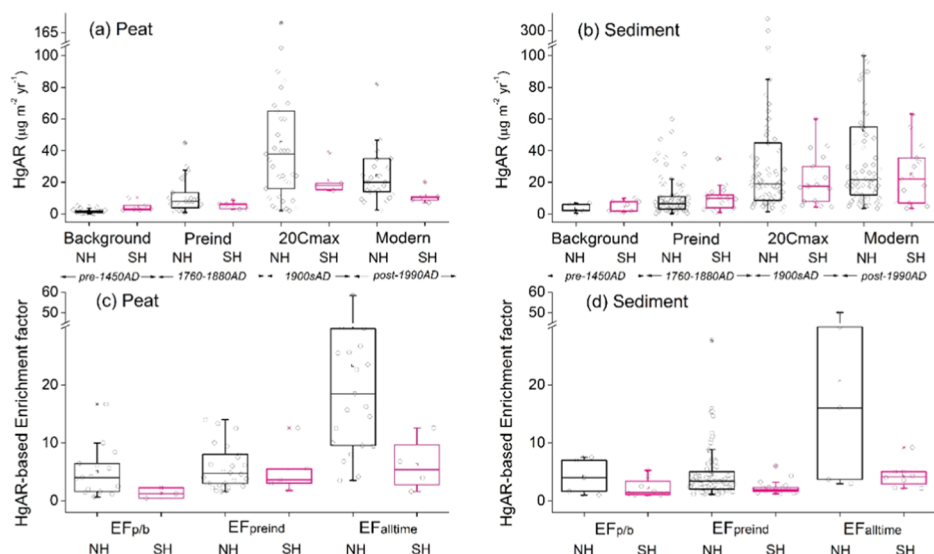


Figure 2. Review of published Hg accumulation rates (HgAR) and enrichment factors (EF) in NH and SH peat and sediment cores for different reference time periods. HgAR ($\mu\text{g m}^{-2} \text{ year}^{-1}$) and EF in peat (a, c) and sediment (b, d) profiles during different periods: Natural background (pre-1450 AD), pre-industrial (1450–1880 AD), extended 20th-century maximum (20Cmax), defined as the broad 20th-century HgAR peak, and modern period (post-1990 AD). $EF_{\text{p/b}}$: EF from natural background to pre-industrial period. EF_{preind} : EF from pre-industrial to 20Cmax. EF_{alltime} : EF from natural background to 20Cmax.

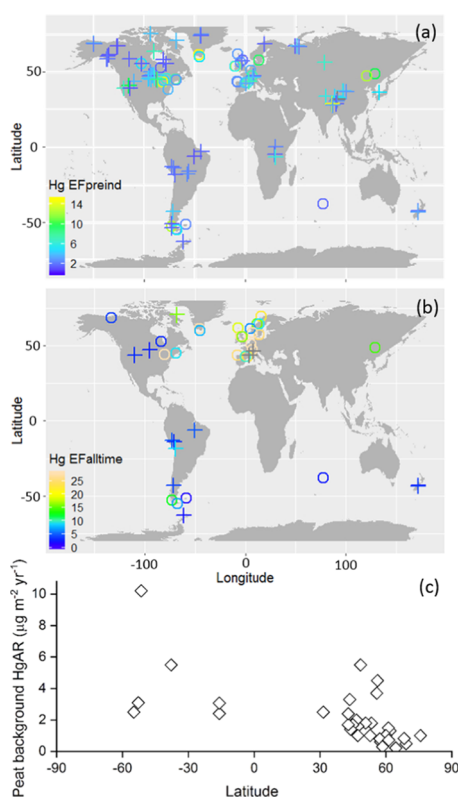


Figure 3. Hg enrichment factors between different reference time periods and peat background Hg accumulation rate. Enrichment factors (EF) in Hg accumulation rates for (a) 20th-century industrial relative to pre-industrial periods ($EF_{pre-ind}$, 1450–1880 AD); (b) 20th-century industrial relative to natural background periods ($EF_{alltime}$, pre-1450 AD century). The circles represent peat cores, and the crosses represent sediment cores. (c) Natural background Hg accumulation rate (pre-1450 AD HgAR) in peat cores as a function of latitude. For details, see [Extended Data 2](#).

this in detail. In summary, our findings, based on combined sediment and peat archive HgAR observations, suggest that all-time atmospheric Hg enrichment during the 20Cmax period (1940–1990) reached 11-fold globally ($EF_{alltime} = 4–24$, 25%–75% quartiles, $n = 39$), 16-fold in the NH ($EF_{alltime} = 10–30$, 25%–75% quartiles, $n = 26$), and 4-fold in the SH ($EF_{alltime} = 2–6$, 25%–75% quartiles, $n = 13$). Atmospheric Hg concentrations decreased from the 1970s to the 2000s by a factor of about 2, a trend that is recorded in the peat archive

HgAR (Figures S4 and S6). Natural background to modern period (1990–2010) Hg enrichment, $EF_{mod/bck}$ based on peat archives, is currently 10-fold globally (± 7.7 , 1σ , $n = 18$), 12 in the NH (± 7.5 , 1σ , $n = 14$), and 3 in the SH (± 2.5 , 1σ , $n = 4$).

Natural and Anthropogenic Hemispheric Hg Emissions. In the following sections, we will further discuss this sizable difference in hemispheric $EF_{alltime}$ in terms of NH and SH Hg emissions and in terms of natural background HgAR. The all-time NH and SH enrichment factors, based on Hg deposition to natural archives, can be directly compared to independent estimates of NH and SH emission factors, i.e., $EF_{emission}$, the ratio of primary, i.e., first time, total Hg emission flux to natural Hg emission flux ($EF_{emission} = F_{anthro} + F_{natural} / F_{natural}$; Table 3). Streets et al. estimated global anthropogenic

Table 3. Summary of Natural and Anthropogenic Hg Emissions to the Atmosphere (Mean $\pm 1\sigma$)

	NH	1σ	SH	1σ
passive volcanic degassing (this study), $Mg\ year^{-1}$	92	20	87	19
eruptive volcanic degassing (this study), $Mg\ year^{-1}$	10	10	10	10
crustal degassing, ^{57,58} $Mg\ year^{-1}$	91	27	44	13
anthropogenic 20Cmax emissions, ⁷ $Mg\ year^{-1}$	2000	500	480	20
mean $EF_{emission}$	11.2	4.6	4.4	1.5
median $EF_{alltime}$	16.1	10–30 IQR	4.0	2–6 IQR

Hg emissions to the atmosphere of $2.4 \pm 0.5\ Gg\ year^{-1}$ during the 20Cmax period (1940–1990).⁷ Natural Hg emissions are the sum of volcanic degassing and crustal degassing from naturally enriched soils. Passive, noneruptive, volcanic degassing is an important direct natural source of Hg to the atmosphere, with a previously estimated total flux of $76 \pm 30\ Mg\ year^{-1}$ (1σ) based on observed Hg/SO₂ ratios of $7.8 \pm 1.5 \times 10^{-6}$ and a global passive degassing SO₂ flux of $9.7\ Tg\ year^{-1}$.^{54,55} Recent advances in remote sensing of SO₂ from 2005 to 2015 indicate a higher SO₂ flux of $23.0 \pm 2.3\ Tg\ year^{-1}$ (1σ),⁵⁶ which we use here to revise the global passive volcanic degassing Hg flux to $179 \pm 39\ Mg\ year^{-1}$ (1σ). Eruptive volcanic SO₂ emissions are indicated to be 1 order of magnitude smaller than passive degassing at $2.6 \pm 2.6\ Tg\ year^{-1}$.⁵⁶ Assuming similar Hg/SO₂ ratios, we estimate eruptive volcanic Hg emissions at $20 \pm 20\ Mg\ year^{-1}$ and total volcanic Hg emissions as the sum of eruptive and passive emissions at

Table 2. Summary of Hg Accumulation Rate (HgAR) Enrichment Factors (EF) in Global Peat and Sediment Records^{a,b}

	pre-ind/background ($EF_{p/b}$)		20Cmax/pre-ind (EF_{preind})		20Cmax/background ($EF_{alltime}$)		modern/background ($EF_{mod/bck}$)	
global-sediment	1.6	$n = 13$	2.9	$n = 103$	4.3	$n = 14$	5.0	$n = 10$
global-peat	2.5	$n = 17$	4.3	$n = 30$	14.5	$n = 25$	10.3	$n = 18$
NH-sediment + peat	3.9	$n = 18$	3.3	$n = 110$	16.1	$n = 26$	10.5	$n = 17$
SH-sediment + peat	1.3	$n = 11$	1.9	$n = 21$	4.0	$n = 13$	3.5	$n = 11$
NH-sediment	3.7	$n = 5$	3.1	$n = 84$	12.8	$n = 5$	19.3	$n = 4$
NH-peat	3.9	$n = 14$	4.6	$n = 25$	16.2	$n = 21$	12.3	$n = 14$
SH-sediment	1.4	$n = 8$	1.8	$n = 17$	3.8	$n = 97$	5.0	$n = 8$
SH-peat	1.2	$n = 3$	3.1	$n = 4$	6.0	$n = 4$	3.1	$n = 4$

^a“Pre-ind,” pre-industrial; “20Cmax,” extended 20th-century maximum HgAR (see [Materials and Methods](#)); “p/b,” pre-industrial/background; “modern/back,” “modern/background”; NH, Northern Hemisphere; SH, Southern Hemisphere. ^bThe number of records, n , do not always add up due to the 2σ outlier tests applied, for, e.g., SH sediment, $n = 8$, SH peat, $n = 3$, but SH sediment + peat, $n = 10$. See [Materials and Methods](#) and [Extended Data 2](#) for details on outlier tests.

$200 \pm 60 \text{ Mg year}^{-1}$ (1σ). Global emissions from naturally enriched soils can be estimated from reviews of flux chamber and soil Hg studies^{57,58} and equal $135 \pm 40 \text{ Mg year}^{-1}$ (1σ , Table 3). These estimates indicate that global anthropogenic 20Cmax Hg emissions of 2.4 Gg year^{-1} have been 7.3 times larger than global natural Hg emissions of $0.34 \text{ Gg year}^{-1}$ and result in a global $\text{EF}_{\text{emission}}$ of 8.2. Volcanic SO_2 emissions are similar for the NH and SH (11.8 vs $11.2 \text{ Tg year}^{-1}$),⁵⁶ leading to NH and SH Hg emission budgets of 0.1 Gg year^{-1} each. We scale naturally enriched soil emissions with continental surface area, to estimate 91 and 44 Mg year^{-1} in NH and SH, respectively. The 20Cmax 2.4 Gg year^{-1} global anthropogenic Hg emissions to the atmosphere were released for 80% to the NH and 20% to the SH.⁷ We therefore estimate hemispheric $\text{EF}_{\text{emission}}$ for the NH at 11.2 ± 4.6 and for the SH at 4.4 ± 1.5 (1σ). The SH $\text{EF}_{\text{emission}}$ of 4.4 is in good agreement with the natural archive-based SH $\text{EF}_{\text{alltime}}$ of 4. The NH $\text{EF}_{\text{emission}}$ of 11, however, underestimates the NH $\text{EF}_{\text{alltime}}$ of 16 by 43%, suggesting that either the $2.0 \pm 0.5 \text{ Gg year}^{-1}$ NH anthropogenic Hg emissions to air⁷ are underestimated, or that the NH natural primary emissions of $91 \pm 27 \text{ Mg year}^{-1}$ are overestimated, or that interhemispheric exchange has transported NH anthropogenic Hg to the SH. There is a final caveat in this analysis that deserves a mention. We assume that the ill-constrained, but potentially important, submarine volcanic Hg flux⁵⁹ is locally or regionally deposited to marine sediments before any of it can be emitted to the atmosphere. This assumption is based on evidence for Hg scavenging in submarine hydrothermal plumes.^{60,61}

The most recent 2018 UNEP global Hg assessment, which provides the state of the science basis for the implementation of the UNEP Minamata Convention on mercury, states that “Human activities have increased total atmospheric Hg concentrations by about 450% (i.e., a factor 4.5) above natural levels.”¹⁴ Our findings therefore suggest that modern (1990–2010) atmospheric Hg enrichment is larger, 10-fold globally. In addition, we find consistently lower anthropogenic Hg enrichment in emissions and in deposition in the SH compared to the NH.

Hemispheric Differences in Hg Deposition and Cycling. The important difference in NH and SH $\text{EF}_{\text{alltime}}$ is not only related to hemispheric differences in primary Hg emissions but also to differences in natural background atmospheric Hg concentrations and HgAR. A notable outcome of the new SH peat records is that the natural SH background HgAR of $4.3 \mu\text{g m}^{-2} \text{ year}^{-1}$ in the SH mid-latitudes (30 – 60°S) is $\times 2.5$ higher than the NH background HgAR of $1.7 \mu\text{g m}^{-2} \text{ year}^{-1}$ in the NH mid-latitudes (Kruskal–Wallis test, $P = 0.02$, Figures 2a, 3c, and S3). Recent Hg stable isotope work on Hg deposition to vegetation and soils suggests that 75% derives from direct uptake of atmospheric Hg(0), and less from Hg(II) wet deposition.^{23,25,62,63} Consequently, peat vegetation Hg(0) uptake is primarily driven by atmospheric Hg(0) concentration and primary productivity.²⁵ Peat vegetation primary productivity depends on climate, which, at the NH and SH mid-latitude sites we study and review, shows similar mean annual air temperatures (NH, 6.7 ; SH, 6.3 °C), precipitation (NH, 1110 ; SH, $1120 \text{ mm year}^{-1}$), and cloud cover (NH, 72 ; SH 77%).⁶⁴ We therefore suggest that the marked NH/SH mid-latitude difference in HgAR is driven by $\times 2.5$ higher natural atmospheric Hg concentrations in the SH, rather than climate factors. Climate factors, such as temperature and length of growth season, only become visible in NH high latitude

($>60^\circ\text{N}$), where HgAR are limited by peat bog primary productivity via the vegetation Hg⁰ pump.²⁴ The observation that the SH natural background HgAR is $\times 2.5$ higher than the NH background is likely an additional reason why the NH $\text{EF}_{\text{alltime}}$ of 16 is much larger than the SH $\text{EF}_{\text{alltime}}$ of 4.

Interhemispheric trends in atmospheric Hg have been previously investigated.^{65,66} Observed mean atmospheric Hg⁰ concentrations across monitoring networks for the modern, 1990–2010 period were 1.8 ng m^{-3} in the NH and 1.2 ng m^{-3} in the SH.^{67,68} Modern-day SH Hg⁰ concentrations are therefore higher than what would be expected based on the estimates of modern NH and SH primary Hg emissions of 1.6 and 0.7 Gg year^{-1} (Table 3). Interhemispheric transport of NH Hg⁰ to the SH potentially contributes to the high SH Hg⁰ concentrations. A key difference between the NH and SH is the land–ocean distribution, with the SH being only 19% land-covered and the NH 39%. The land–ocean distribution plays an important role in atmospheric boundary layer Hg dynamics. A study on atmospheric Hg⁰ seasonality, which is more pronounced in the NH and quasi-absent in the SH, suggested that the vegetation Hg pump, i.e., the foliar uptake of Hg⁰ and sequestration in soils, is an important driver of NH atmospheric Hg⁰ seasonality.²⁴ The SH has a smaller terrestrial vegetation and soil pool, and we speculate that the SH has relatively higher atmospheric Hg⁰ due to a weaker vegetation Hg pump. In addition, coupled ocean–atmosphere Hg chemistry and transport models find stronger marine Hg⁰ evasion in the SH than in the NH, mainly due to upwelling of Hg-rich deep waters in the Southern Ocean.^{19,69} The model studies suggest that SH atmospheric Hg⁰ is largely controlled by these SH marine Hg⁰ emissions.^{8,19} These findings were recently confirmed by long-term observations on Hg⁰ seasonality at the Cape Point monitoring station in South Africa.⁷⁰ The 2-fold higher SH natural background HgAR in peat therefore echoes the higher-than-expected modern SH atmospheric Hg⁰ concentrations, and both can potentially be explained by the hemispheric land–ocean distribution.

We use peat $\text{EF}_{\text{mod/bck}}$ for both hemispheres (Table 2) to estimate what natural atmospheric Hg⁰ concentrations may have been during pre-1450 AD times. Dividing modern-day mean NH and SH atmospheric Hg⁰ concentrations of 1.8 and 1.2 ng m^{-3} by $\text{EF}_{\text{mod/bck}}$ yields natural background atmospheric Hg concentrations of 0.2 and 0.4 ng m^{-3} for the NH and SH. In summary, the lower SH enrichment in atmospheric Hg appears to be caused by a combination of lower SH anthropogenic Hg emissions and higher SH background Hg concentrations. We speculate that the higher SH atmospheric background is driven by a lower SH land/ocean ratio, which limits the terrestrial vegetation Hg pump and sustains higher natural marine Hg emissions. Overall, our findings suggest that both background Hg concentrations and all-time Hg enrichment in the NH and SH are different and should be taken into account in environmental policy objectives.

■ ASSOCIATED CONTENT

Supporting Information

The Supporting Information is available free of charge at <https://pubs.acs.org/doi/10.1021/acsearthspacechem.0c00220>.

Details of the coring sites in this investigation (Table S1); location of Amsterdam Island (AMS), Falkland Islands (SCB, Islas Malvinas), Andorra (AND), and

Harberton (HBT) (Figure S1); accelerator mass spectrometry ^{14}C dating of plant macrofossils from all of the four peat cores (Table S2); age models of peat cores from AMS, SCB, AND, and HBT using Bacon (Figure S2); summary of Hg measurements in standard reference materials (Table S3); natural background Hg accumulation rates (Figure S3); profiles of HgAR enrichment factor (Figure S4); profiles of Hg concentration (Figure S5); and historical atmospheric Hg monitoring observations and reconstructed Hg levels (Figure S6) (PDF)

Extended Data 1 (XLSX)

Extended Data 2 (XLSX)

All data generated or analyzed during this study are included in this published article (and its SI Appendix).

AUTHOR INFORMATION

Corresponding Author

Jeroen E. Sonke – *Laboratoire Géosciences Environnement Toulouse, Université de Toulouse, CNRS, IRD, UPS, Toulouse 31400, France*; orcid.org/0000-0001-7146-3035; Email: jeroen.sonke@get.omp.eu

Authors

Chuxian Li – *Laboratoire Écologie Fonctionnelle et Environnement, Université de Toulouse, CNRS, Toulouse 31326, France*; *Laboratoire Géosciences Environnement Toulouse, Université de Toulouse, CNRS, IRD, UPS, Toulouse 31400, France*

Gaël Le Roux – *Laboratoire Écologie Fonctionnelle et Environnement, Université de Toulouse, CNRS, Toulouse 31326, France*; orcid.org/0000-0002-1579-0178

Natalia Piotrowska – *Institute of Physics—CSE, Silesian University of Technology, 44-100 Gliwice, Poland*

Nathalie Van der Putten – *Faculty of Science, Vrije Universiteit Amsterdam, 1081 HV Amsterdam, The Netherlands*

Stephen J. Roberts – *British Antarctic Survey, Cambridge CB3 0ET, U.K.*

Tim Daley – *School of Geography, Earth and Environmental Sciences, Plymouth University, Plymouth PL4 8AA, U.K.*

Emma Rice – *School of Geography, Earth and Environmental Sciences, Plymouth University, Plymouth PL4 8AA, U.K.*

Roland Gehrels – *Department of Environment & Geography, University of York, York YO10 5NG, U.K.*

Maxime Enrico – *Laboratoire Écologie Fonctionnelle et Environnement, Université de Toulouse, CNRS, Toulouse 31326, France*; *Laboratoire Géosciences Environnement Toulouse, Université de Toulouse, CNRS, IRD, UPS, Toulouse 31400, France*; *Harvard John A. Paulson School of Engineering & Applied Sciences, Harvard University, Cambridge, Massachusetts 02138, United States*

Dmitri Mauquoy – *Geography and Environment, School of Geosciences, University of Aberdeen, Aberdeen AB24 3UF, U.K.*

Thomas P. Roland – *Geography, College of Life and Environmental Sciences, University of Exeter, Exeter EX4 4RJ, U.K.*

François De Vleeschouwer – *Instituto Franco-Argentino para el Estudio delClima y sus Impactos (UMI 3351 IFAECI/ CNRS-CONICET-UBA), Universidad de Buenos Aires, Buenos Aires C1053 CABA, Argentina*

Complete contact information is available at:

<https://pubs.acs.org/10.1021/acsearthspacechem.0c00220>

Author Contributions

J.E.S. and F.D.V. initiated and designed the project. All authors were involved in field sampling, laboratory analyses, and/or data analysis. C.L. and J.E.S. wrote the manuscript on which all authors commented.

Notes

The authors declare no competing financial interest.

ACKNOWLEDGMENTS

Field work was funded by the French Polar Institute (IPEV, Brest, France) through the IPEV Programmes 1066 “PARAD” (to F.D.V.) and 1065 PALATIO (to N.V.P. and E. Michel). J.E.S. acknowledges funding from the H2020 ERA-PLANET (689443) iGOSP and iCUPE programs. The authors thank the South Atlantic Environmental Research Institute (SAERI) for providing laboratory facilities in the Falkland Islands and E. Brook (Falkland Islands Government Training Centre) for logistical support. They are grateful to N. Marchand (IPEV) for the logistical support, C. Marteau for making the sampling possible in very restricted areas of the TAAF Nature Reserve, and N. Roberts for help processing the San Carlos core and scientific discussions. They thank A. Coronato, R. López, and V. Pancotto from CADIC-CONICET (Ushuaia) for the field campaigns in Andorra and Harberton. Radiocarbon ages were obtained as part of the IDEX Peat3 project of the University of Toulouse and through the national service support: Artemis-INSU-CNRS (to G.L.R.). C.L.’s PhD is supported by a scholarship from the China Scholarship Council. The authors thank 12 anonymous reviewers for their constructive comments on the various versions of this paper, and editor J. D. Blum for handling the final version.

REFERENCES

- (1) Outridge, P. M.; Mason, R. P.; Wang, F.; Guerrero, S.; Heimbürger-Boavida, L. E. Updated Global and Oceanic Mercury Budgets for the United Nations Global Mercury Assessment 2018. *Environ. Sci. Technol.* **2018**, *52*, 11466–11477.
- (2) Mason, R. P.; Choi, A. L.; Fitzgerald, W. F.; Hammerschmidt, C. R.; Lamborg, C. H.; Soerensen, A. L.; Sunderland, E. M. Mercury Biogeochemical Cycling in the Ocean and Policy Implications. *Environ. Res.* **2012**, *119*, 101–117.
- (3) Chen, C.; Amirbahman, A.; Fisher, N.; Harding, G.; Lamborg, C.; Nacci, D.; Taylor, D. Methylmercury in Marine Ecosystems: Spatial Patterns and Processes of Production, Bioaccumulation, and Biomagnification. *EcoHealth* **2008**, *5*, 399–408.
- (4) Sunderland, E. M. Mercury Exposure from Domestic and Imported Estuarine and Marine Fish in the U.S. Seafood Market. *Environ. Health Perspect.* **2007**, *115*, 235–242.
- (5) Pirrone, N.; Cinnirella, S.; Feng, X.; Finkelman, R. B.; Friedli, H. R.; Leaner, J.; Mason, R.; Mukherjee, A. B.; Stracher, G. B.; Streets, D. G.; Telmer, K. Global Mercury Emissions to the Atmosphere from Anthropogenic and Natural Sources. *Atmos. Chem. Phys.* **2010**, *10*, 5951–5964.
- (6) Pacyna, E. G.; Pacyna, J. M.; Sundseth, K.; Munthe, J.; Kindbom, K.; Wilson, S.; Steenhuisen, F.; Maxson, P. Global Emission of Mercury to the Atmosphere from Anthropogenic Sources in 2005 and Projections to 2020. *Atmos. Environ.* **2010**, *44*, 2487–2499.
- (7) Streets, D. G.; Horowitz, H. M.; Jacob, D. J.; Lu, Z.; Levin, L.; ter Schure, A. F. H.; Sunderland, E. M. Total Mercury Released to the Environment by Human Activities. *Environ. Sci. Technol.* **2017**, *51*, 5969–5977.
- (8) Horowitz, H. M.; Jacob, D. J.; Zhang, Y.; Dibble, T. S.; Slemr, F.; Amos, H. M.; Schmidt, J. A.; Corbitt, E. S.; Marais, E. A.; Sunderland, E. M. A New Mechanism for Atmospheric Mercury Redox Chemistry:

- Implications for the Global Mercury Budget. *Atmos. Chem. Phys.* **2017**, *17*, 6353–6371.
- (9) Engstrom, D. R.; Fitzgerald, W. F.; Cooke, C. A.; Lamborg, C. H.; Drevnick, P. E.; Swain, E. B.; Balogh, S. J.; Balcom, P. H. Atmospheric Hg Emissions from Preindustrial Gold and Silver Extraction in the Americas: A Reevaluation from Lake-Sediment Archives. *Environ. Sci. Technol.* **2014**, *48*, 6533–6543.
- (10) Fitzgerald, W. F.; Engstrom, D. R.; Mason, R. P.; Nater, E. A. The Case for Atmospheric Mercury Contamination in Remote Areas. *Environ. Sci. Technol.* **1998**, *32*, 1–7.
- (11) Martínez-Cortizas, A. Mercury in a Spanish Peat Bog: Archive of Climate Change and Atmospheric Metal Deposition. *Science* **1999**, *284*, 939–942.
- (12) Schuster, P. F.; Krabbenhoft, D. P.; Naftz, D. L.; Cecil, L. D.; Olson, M. L.; Dewild, J. F.; Susong, D. D.; Green, J. R.; Abbott, M. L. Atmospheric Mercury Deposition during the Last 270 Years: A Glacial Ice Core Record of Natural and Anthropogenic Sources. *Environ. Sci. Technol.* **2002**, *36*, 2303–2310.
- (13) Thomas, R. L. The Distribution of Mercury in the Sediments of Lake Ontario. *Can. J. Earth Sci.* **1972**, *9*, 636–651.
- (14) UNEP. *Global Mercury Assessment 2018*; 2018.
- (15) Fitzgerald, W. F.; Engstrom, D. R.; Mason, R. P.; Nater, E. A. The Case for Atmospheric Mercury Contamination in Remote Areas. *Environ. Sci. Technol.* **1998**, *32*, 1–7.
- (16) Engstrom, D. R.; Fitzgerald, W. F.; Cooke, C. A.; Lamborg, C. H.; Drevnick, P. E.; Swain, E. B.; Balogh, S. J.; Balcom, P. H. Atmospheric Hg Emissions from Preindustrial Gold and Silver Extraction in the Americas: A Reevaluation from Lake-Sediment Archives. *Environ. Sci. Technol.* **2014**, *48*, 6533–6543.
- (17) Biester, H.; Bindler, R.; Martínez-Cortizas, A.; Engstrom, D. R. Modeling the Past Atmospheric Deposition of Mercury Using Natural Archives. *Environ. Sci. Technol.* **2007**, *41*, 4851–4860.
- (18) Amos, H. M.; Sonke, J. E.; Obrist, D.; Robins, N.; Hagan, N.; Horowitz, H. M.; Mason, R. P.; Witt, M.; Hedgecock, I. M.; Corbitt, E. S.; Sunderland, E. M. Observational and Modeling Constraints on Global Anthropogenic Enrichment of Mercury. *Environ. Sci. Technol.* **2015**, *49*, 4036–4047.
- (19) Zhang, Y.; Jaeglé, L.; Thompson, L.; Streets, D. G. Six Centuries of Changing Oceanic Mercury: Anthropogenic Mercury in Ocean. *Global Biogeochem. Cycles* **2014**, *28*, 1251–1261.
- (20) Biester, H.; Bindler, R.; Martínez-Cortizas, A.; Engstrom, D. R. Modeling the Past Atmospheric Deposition of Mercury Using Natural Archives. *Environ. Sci. Technol.* **2007**, *41*, 4851–4860.
- (21) Cooke, C. A.; Hobbs, W. O.; Michelutti, N.; Wolfe, A. P. Reliance on Pb-210 Chronology Can Compromise the Inference of Preindustrial Hg Flux to Lake Sediments. *Environ. Sci. Technol.* **2010**, *44*, 1998–2003.
- (22) Abril, J. M.; Brunskill, G. Evidence That Excess ^{210}Pb Flux Varies with Sediment Accumulation Rate and Implications for Dating Recent Sediments. *J. Paleolimnol.* **2014**, *52*, 121–137.
- (23) Enrico, M.; Roux, G. L.; Maruszczak, N.; Heimbürger, L.-E.; Claustres, A.; Fu, X.; Sun, R.; Sonke, J. E. Atmospheric Mercury Transfer to Peat Bogs Dominated by Gaseous Elemental Mercury Dry Deposition. *Environ. Sci. Technol.* **2016**, *50*, 2405–2412.
- (24) Jiskra, M.; Sonke, J. E.; Obrist, D.; Bieser, J.; Ebinghaus, R.; Myhre, C. L.; Pfaffhuber, K. A.; Wängberg, I.; Kyllönen, K.; Worthy, D.; Martin, L. G.; Labuschagne, C.; Mkololo, T.; Ramonet, M.; Magand, O.; Dommergue, A. A Vegetation Control on Seasonal Variations in Global Atmospheric Mercury Concentrations. *Nat. Geosci.* **2018**, *11*, 244–250.
- (25) Enrico, M.; Le Roux, G.; Heimbürger, L.-E.; Van Beek, P.; Souhaut, M.; Chmieleff, J.; Sonke, J. E. Holocene Atmospheric Mercury Levels Reconstructed from Peat Bog Mercury Stable Isotopes. *Environ. Sci. Technol.* **2017**, *51*, 5899–5906.
- (26) European Monitoring and Evaluation Programme. <https://www.emep.int/>; 2016.
- (27) Streets, D. G.; Devane, M. K.; Lu, Z.; Bond, T. C.; Sunderland, E. M.; Jacob, D. J. All-Time Releases of Mercury to the Atmosphere from Human Activities. *Environ. Sci. Technol.* **2011**, *45*, 10485–10491.
- (28) Streets, D. G.; Horowitz, H. M.; Lu, Z.; Levin, L.; Thackray, C. P.; Sunderland, E. M. Five Hundred Years of Anthropogenic Mercury: Spatial and Temporal Release Profiles. *Environ. Res. Lett.* **2019**, *14*, No. 084004.
- (29) Amos, H. M.; Jacob, D. J.; Streets, D. G.; Sunderland, E. M. Legacy Impacts of All-Time Anthropogenic Emissions on the Global Mercury Cycle: Global Impacts Of Legacy Mercury. *Global Biogeochem. Cycles* **2013**, *27*, 410–421.
- (30) Cooke, C. A.; Hintelmann, H.; Ague, J. J.; Burger, R.; Biester, H.; Sachs, J. P.; Engstrom, D. R. Use and Legacy of Mercury in the Andes. *Environ. Sci. Technol.* **2013**, *47*, 4181–4188.
- (31) Streets, D. G.; Horowitz, H. M.; Jacob, D.; Lu, Z.; Levin, L.; ter Schure, A. F. H.; Sunderland, E. M. Total Mercury Released to the Environment by Human Activities. *Environ. Sci. Technol.* **2017**, *51*, 5969–5977.
- (32) Amos, H. M.; Sonke, J. E.; Obrist, D.; Robins, N.; Hagan, N.; Horowitz, H. M.; Mason, R. P.; Witt, M.; Hedgecock, I. M.; Corbitt, E. S.; Sunderland, E. M. Observational and Modeling Constraints on Global Anthropogenic Enrichment of Mercury. *Environ. Sci. Technol.* **2015**, *49*, 4036–4047.
- (33) Cooke, C. A.; Martínez-Cortizas, A.; Bindler, R.; Gustin, M. S. Environmental Archives of Atmospheric Hg Deposition – A Review. *Sci. Total Environ.* **2020**, *709*, No. 134800.
- (34) Lindberg, S.; Bullock, R.; Ebinghaus, R.; Engstrom, D.; Feng, X.; Fitzgerald, W.; Pirrone, N.; Prestbo, E.; Seigneur, C. A Synthesis of Progress and Uncertainties in Attributing the Sources of Mercury Deposition. *Ambio* **2007**, *36*, 19–32.
- (35) Biester, H.; Kilian, R.; Franzen, C.; Woda, C.; Mangini, A.; Schöler, H. F. Elevated Mercury Accumulation in a Peat Bog of the Magellanic Moorlands, Chile (53°S) – an Anthropogenic Signal from the Southern Hemisphere. *Earth Planet. Sci. Lett.* **2002**, *201*, 609–620.
- (36) Guédon, S.; Ledru, M.-P.; Escobar-Torrez, K.; Develle, A. L.; Brisset, E. Enhanced Mercury Deposition by Amazonian Orographic Precipitation: Evidence from High-Elevation Holocene Records of the Lake Titicaca Region (Bolivia). *Palaeogeogr. Palaeoclimatol. Palaeoecol.* **2018**, *511*, 577–587.
- (37) Le Roux, G.; Vleeschouwer, F. Preparation of Peat Samples for Inorganic Geochemistry Used as Palaeoenvironmental Proxies. *Mires Peat* **2011**, *7*, 1–9.
- (38) Givélet, N.; Le Roux, G.; Cheburkin, A.; Chen, B.; Frank, J.; Goodsite, M.; Kempter, H.; Krachler, M.; Noernberg, T.; Rausch, N.; Rheinberger, S.; Roos-Barraclough, F.; Sapkota, A.; Scholz, C.; Shoty, W. Suggested Protocol for Collecting, Handling and Preparing Peat Cores and Peat Samples for Physical, Chemical, Mineralogical and Isotopic Analyses. *J. Environ. Monit.* **2004**, *6*, 481–492.
- (39) Li, C.; Sonke, J. E.; Le Roux, G.; Van der Putten, N.; Piotrowska, N.; Jeandel, C.; Mattielli, N.; Benoit, M.; Wiggs, G. F. S.; De Vleeschouwer, F. Holocene Dynamics of the Southern Westerly Winds over the Indian Ocean Inferred from a Peat Dust Deposition Record. *Quat. Sci. Rev.* **2020**, *231*, No. 106169.
- (40) Goodsite, M. E.; Rom, W.; Heinemeier, J.; Lange, T.; Ooi, S.; Appleby, P. G.; Shoty, W.; van der Knaap, W. O.; Lohse, C.; Hansen, T. S. High-Resolution AMS ^{14}C Dating of Post-Bomb Peat Archives of Atmospheric Pollutants. *Radiocarbon* **2001**, *43*, 495–515.
- (41) Appleby, P. G. Chronostratigraphic Techniques in Recent Sediments. In *Tracking Environmental Change Using Lake Sediments*; Last, W. M.; Smol, J. P., Eds.; Kluwer Academic Publishers: Dordrecht, 2002; Vol. 1, pp 171–203.
- (42) Piotrowska, N. Status Report of AMS Sample Preparation Laboratory at GADAM Centre, Gliwice, Poland. *Nucl. Instrum. Methods Phys. Res., Sect. B* **2013**, *294*, 176–181.
- (43) Zoppi, U.; Crye, J.; Song, Q.; Arjomand, A. Performance Evaluation of the New AMS System at Accium BioSciences. *Radiocarbon* **2007**, *49*, 171–180.
- (44) Davies, L. J.; Appleby, P.; Jensen, B. J. L.; Magnan, G.; Mullan-Boudreau, G.; Noernberg, T.; Shannon, B.; Shoty, W.; van Bellen, S.; Zaccane, C.; Froese, D. G. High-Resolution Age Modelling of Peat Bogs from Northern Alberta, Canada, Using Pre- and Post-Bomb

- 14C, 210Pb and Historical Cryptotephra. *Quat. Geochronol.* **2018**, *47*, 138–162.
- (45) Blaauw, M.; Christen, J. A. Flexible Paleoclimate Age-Depth Models Using an Autoregressive Gamma Process. *Bayesian Anal.* **2011**, *6*, 457–474.
- (46) Hogg, A. G.; Hua, Q.; Blackwell, P. G.; Niu, M.; Buck, C. E.; Guilderson, T. P.; Heaton, T. J.; Palmer, J. G.; Reimer, P. J.; Reimer, R. W.; Turney, C. S. M.; Zimmerman, S. R. H. SHCal13 Southern Hemisphere Calibration, 0–50,000 Years Cal BP. *Radiocarbon* **2013**, *55*, 1889–1903.
- (47) Hua, Q.; Barbetti, M.; Rakowski, A. Z. Atmospheric Radiocarbon for the Period 1950–2010. *Radiocarbon* **2013**, *55*, 2059–2072.
- (48) Lamborg, C. H.; Fitzgerald, W. F.; Damman, A. W. H.; Benoit, J. M.; Balcom, P. H.; Engstrom, D. R. Modern and Historic Atmospheric Mercury Fluxes in Both Hemispheres: Global and Regional Mercury Cycling Implications: Modern and Historic Fluxes of Atmospheric Mercury. *Global Biogeochem. Cycles* **2002**, *16*, 51–1–51–11.
- (49) Cooke, C. A.; Balcom, P. H.; Kerfoot, C.; Abbott, M. B.; Wolfe, A. P. Pre-Columbian Mercury Pollution Associated with the Smelting of Argentiferous Ores in the Bolivian Andes. *Ambio* **2011**, *40*, 18–25.
- (50) Ribeiro Guevara, S.; Meili, M.; Rizzo, A.; Daga, R.; Arribé, M. Sediment Records of Highly Variable Mercury Inputs to Mountain Lakes in Patagonia during the Past Millennium. *Atmos. Chem. Phys.* **2010**, *10*, 3443–3453.
- (51) Cooke, C. A.; Balcom, P. H.; Biester, H.; Wolfe, A. P. Over Three Millennia of Mercury Pollution in the Peruvian Andes. *Proc. Natl. Acad. Sci. U.S.A.* **2009**, *106*, 8830–8834.
- (52) Guerero, S. Chemistry as a Tool for Historical Research: Identifying Paths of Historical Mercury Pollution in the Hispanic New World. *Bull. Hist. Chem.* **2012**, *37*, 61–70.
- (53) Roser, M.; Ritchie, H.; Ortiz-Ospina, E. World Population Growth. <https://Ourworldindata.org/World-Population-Growth>; 2013.
- (54) Bagnato, E.; Tamburello, G.; Avar, G.; Martinez-Cruz, M.; Enrico, M.; Fu, X.; Sprovieri, M.; Sonke, J. E. Mercury Fluxes from Volcanic and Geothermal Sources: An Update. *Geol. Soc. London, Spec. Publ.* **2015**, *410*, 263–285.
- (55) Andres, R. J.; Kasgnoc, A. D. A Time-Averaged Inventory of Subaerial Volcanic Sulfur Emissions. *J. Geophys. Res.* **1998**, *103*, 25251–25261.
- (56) Carn, S. A.; Fioletov, V. E.; McLinden, C. A.; Li, C.; Krotkov, N. A. A Decade of Global Volcanic SO₂ Emissions Measured from Space. *Sci. Rep.* **2017**, *7*, No. 44095.
- (57) Kocman, D.; Horvat, M.; Pirrone, N.; Cinnirella, S. Contribution of Contaminated Sites to the Global Mercury Budget. *Environ. Res.* **2013**, *125*, 160–170.
- (58) Agnan, Y.; Le Dantec, T.; Moore, C. W.; Edwards, G. C.; Obrist, D. New Constraints on Terrestrial Surface–Atmosphere Fluxes of Gaseous Elemental Mercury Using a Global Database. *Environ. Sci. Technol.* **2016**, *50*, 507–524.
- (59) Fitzgerald, W. F.; Lamborg, C. H. *Geochemistry of Mercury. In Treatise on Geochemistry: Volume 9: Environmental Geochemistry*; Pergamon: Oxford, 2004.
- (60) Lamborg, C. H.; Von Damm, K. L.; Fitzgerald, W. F.; Hammerschmidt, C. R.; Zierenberg, R. Mercury and Monomethylmercury in Fluids from Sea Cliff Submarine Hydrothermal Field, Gorda Ridge. *Geophys. Res. Lett.* **2006**, *33*, No. L17606.
- (61) Bowman, K. L.; Hammerschmidt, C. R.; Lamborg, C. H.; Swarr, G. J.; Agather, A. M. Distribution of Mercury Species across a Zonal Section of the Eastern Tropical South Pacific Ocean (U.S. GEOTRACES GP16). *Mar. Chem.* **2016**, *186*, 156–166.
- (62) Demers, J. D.; Blum, J. D.; Zak, D. R. Mercury Isotopes in a Forested Ecosystem: Implications for Air-Surface Exchange Dynamics and the Global Mercury Cycle. *Global Biogeochem. Cycles* **2013**, *27*, 222–238.
- (63) Zheng, W.; Obrist, D.; Weis, D.; Bergquist, B. A. Mercury Isotope Compositions across North American Forests: Mercury Isotopes Across U.S. Forests. *Global Biogeochem. Cycles* **2016**, *30*, 1475–1492.
- (64) Hersbach, H.; Bell, B.; Berrisford, P.; Hirahara, S.; Horányi, A.; Muñoz-Sabater, J.; Nicolas, J.; Peubey, C.; Radu, R.; Schepers, D.; Simmons, A.; Soci, C.; Abdalla, S.; Abellan, X.; Balsamo, G.; Bechtold, P.; Biavati, G.; Bidlot, J.; Bonavita, M.; De Chiara, G.; Dahlgren, P.; Dee, D.; Diamantakis, M.; Dragani, R.; Flemming, J.; Forbes, R.; Fuentes, M.; Geer, A.; Haimberger, L.; Healy, S.; Hogan, R. J.; Hólm, E.; Janisková, M.; Keeley, S.; Laloyaux, P.; Lopez, P.; Lupu, C.; Radnoti, G.; de Rosnay, P.; Rozum, I.; Vamborg, F.; Villaume, S.; Thépaut, J.-N. The ERA5 Global Reanalysis. *Q. J. R. Meteorol. Soc.* **2020**, *146*, 1999–2049.
- (65) Slemr, F.; Seiler, W.; Schuster, G. Latitudinal Distribution of Mercury over the Atlantic Ocean. *J. Geophys. Res.* **1981**, *86*, 1159.
- (66) Bieser, J.; Slemr, F.; Ambrose, J.; Brenninkmeijer, C.; Brooks, S.; Dastoor, A.; DeSimone, F.; Ebinghaus, R.; Gencarelli, C. N.; Geyer, B.; Gratz, L. E.; Hedgecock, I. M.; Jaffe, D.; Kelley, P.; Lin, C.-J.; Jaegle, L.; Matthias, V.; Ryjkov, A.; Selin, N. E.; Song, S.; Travnikov, O.; Weigelt, A.; Luke, W.; Ren, X.; Zahn, A.; Yang, X.; Zhu, Y.; Pirrone, N. Multi-Model Study of Mercury Dispersion in the Atmosphere: Vertical and Interhemispheric Distribution of Mercury Species. *Atmos. Chem. Phys.* **2017**, *17*, 6925–6955.
- (67) Sprovieri, F.; Pirrone, N.; Bencardino, M.; D’Amore, F.; Carbone, F.; Cinnirella, S.; Mannarino, V.; Landis, M.; Ebinghaus, R.; Weigelt, A.; Brunke, E.-G.; Labuschagne, C.; Martin, L.; Munthe, J.; Wängberg, I.; Artaxo, P.; Morais, F.; de Melo Jorge Barbosa, H.; Brito, J.; Cairns, W.; Barbante, C.; del Carmen Diéguez, M.; Garcia, P. E.; Dommergue, A.; Angot, H.; Magand, O.; Skov, H.; Horvat, M.; Kotnik, J.; Read, K. A.; Neves, L. M.; Gawlik, B. M.; Sena, F.; Mashyanov, N.; Obolkin, V.; Wip, D.; Feng, X. B.; Zhang, H.; Fu, X.; Ramachandran, R.; Cossa, D.; Knoery, J.; Maruszczak, N.; Nerentorp, M.; Norstrom, C. Atmospheric Mercury Concentrations Observed at Ground-Based Monitoring Sites Globally Distributed in the Framework of the GMOS Network. *Atmos. Chem. Phys.* **2016**, *16*, 11915–11935.
- (68) Zhang, Y.; Jacob, D. J.; Horowitz, H. M.; Chen, L.; Amos, H. M.; Krabbenhoft, D. P.; Slemr, F.; St. Louis, V. L.; Sunderland, E. M. Observed Decrease in Atmospheric Mercury Explained by Global Decline in Anthropogenic Emissions. *Proc. Natl. Acad. Sci. U.S.A.* **2016**, *113*, 526–531.
- (69) Strode, S. A.; Jaegle, L.; Selin, N. E.; Jacob, D. J.; Park, R. J.; Yantosca, R. M.; Mason, R. P.; Slemr, F. Air-Sea Exchange in the Global Mercury Cycle: Mercury Air-Sea Exchange. *Global Biogeochem. Cycles* **2007**, *21*, No. GB1017.
- (70) Bieser, J.; Angot, H.; Slemr, F.; Martin, L. Atmospheric mercury in the Southern Hemisphere – Part 2: Source apportionment analysis at Cape Point station, South Africa. *Atmos. Chem. Phys.* **2020**, *20*, 10427–10439.